



HAL
open science

Understanding the Cu^{2+} adsorption mechanism on activated carbon using advanced statistical physics modelling

Lotfi Sellaoui, Fatma Dhaouadi, Sonia Taamalli, Florent Louis, Abderrahman El Bakali, Michael Badawi, Adrián Bonilla-Petriciolet, Luis Silva, Kátia da Boit Martinello, Guilherme Luiz Dotto, et al.

► To cite this version:

Lotfi Sellaoui, Fatma Dhaouadi, Sonia Taamalli, Florent Louis, Abderrahman El Bakali, et al.. Understanding the Cu^{2+} adsorption mechanism on activated carbon using advanced statistical physics modelling. *Environmental Science and Pollution Research*, 2022, 29, pp.54882-54889. 10.1007/s11356-022-19795-7. hal-03633260

HAL Id: hal-03633260

<https://hal.science/hal-03633260v1>

Submitted on 19 Jan 2024

HAL is a multi-disciplinary open access archive for the deposit and dissemination of scientific research documents, whether they are published or not. The documents may come from teaching and research institutions in France or abroad, or from public or private research centers.

L'archive ouverte pluridisciplinaire **HAL**, est destinée au dépôt et à la diffusion de documents scientifiques de niveau recherche, publiés ou non, émanant des établissements d'enseignement et de recherche français ou étrangers, des laboratoires publics ou privés.

26 models contain parameters that were utilized to provide new insights into the possible
27 adsorption mechanism at the molecular scale. In particular, a monolayer adsorption model was
28 the best alternative to correlate the Cu^{2+} adsorption data at 25 – 55 °C and pH 5.5. Furthermore,
29 the application of this model for copper adsorption data analysis showed that the removal of this
30 heavy metal ion was a multi-cationic process. This theoretical finding indicated that Cu^{2+} ions
31 interacted via one functional group of activated carbon surface during adsorption. In this
32 direction, the adsorption energy was calculated thus showing that Cu^{2+} removal was endothermic
33 and associated with physical interaction forces. Furthermore, these activated carbons showed
34 saturation adsorption capacities from 54.6 to 87.0 mg/g for Cu^{2+} removal, and their
35 performances outperformed other adsorbents available in the literature. Overall, these results
36 provided new insights of the adsorption mechanism of this water pollutant using activated carbons.

37

38 **Keywords:** Adsorption; Copper; Isotherms; Statistical physics;

39

40 **1. Introduction**

41

42 Copper is a transition metal, electrically and thermally conductive, but it is also considered as
43 an environmental pollutant (Kayalvizhi et al. 2022). Natural disasters (e.g., volcanic phenomena)
44 and anthropogenic activities (e.g., metal industries, tanning factories, and automobile
45 industries) contribute to the pollution caused by copper. This metal is toxic even at relatively
46 low concentrations, and, consequently, the highest permissible concentration level of copper
47 ions (Cu^{2+}) in marine water has been established as 4.8 $\mu\text{g/L}$. In comparison, the maximum Cu^{2+}
48 concentration for drinking water is 1300 $\mu\text{g/L}$, as reported by the WHO and EPA (Katiyar et al.
49 2021; Kayalvizhi et al. 2022). Chronic exposure to this metal can affect vital organs such as the

50 intestines, stomach, and liver. It can also generate diverse symptoms such as liver disease,
51 gallbladder, and metabolic disturbances(Dou et al. 2019; Sun et al. 2022).

52 Consequently, the drinking water resources and effluents polluted with Cu^{2+} must be
53 treated to reduce their concentration thus avoiding environmental impacts and to protect human
54 health. Various procedures have been reported to remove Cu^{2+} ions from liquid phase. They
55 include ion exchange, precipitation, electrolysis, reverse osmosis, flocculation, biochemical
56 methods, and membrane-based filtration (Godiya et al. 2019; Nyström et al. 2020; Anbazhagan
57 et al. 2021; Lemes and Tarley 2021). However, these removal methods have disadvantages such
58 as unfavorable cost-effectiveness tradeoffs or the generation of toxic sediments and wastes(e.g.,
59 sludge)(Rukayat et al. 2021). In contrast, the adsorption process is a competitive technique
60 compared to other methods due to its ease of handling, low cost, and removal efficacy even at
61 low concentrations of heavy metal ions (Vocciante et al. 2014; Pan et al. 2019; Khan et al.
62 2021). Activated carbon is the most employed adsorbent in this process because it effectively
63 removes inorganic and organic pollutants from wastewaters and industrial effluents. This
64 adsorbent outperforms other materials reported for water treatment in terms of its production
65 cost and the availability of a wide spectrum of preparation routes that is already exploited and
66 commercialized at large industrial scale. The adsorption performance of activated carbon is
67 governed by its pore structure and surface chemistry. The modification of activated carbon is
68 aimed to optimize these properties (Bell et al. 2011), and this adsorbent can be obtained from
69 different feedstock and preparation conditions, thus affecting its adsorption properties. Surface
70 functionalization of activated carbons can be performed with several chemicals to tailor their
71 performance for the removal of target pollutants.

72 Under this context, citric wastes can be an option to produce activated carbons since
73 they are generated in large amounts by industries of juices and jams. During the production
74 process of juices and jams, around 50-60% of the entire citric fruit is discarded. These wastes

75 cannot be released into the environment since they generate CH₄. On the other hand, they are
76 rich in lignin, cellulose, hemicellulose, and pectin, thus being an attractive feedstock for
77 pyrolysis and their conversion into activated carbon (Lam et al. 2016, 2018).

78 The modeling of adsorption data of heavy metals and other water pollutants is important
79 for water treatment design. Therefore, it is possible to apply classical models (e.g., Langmuir)
80 to theoretically study the adsorption data. Unfortunately, this and other traditional models are
81 not useful to understand the adsorption mechanisms due to the limitations in their hypotheses.
82 For instance, Langmuir model considers that each functional group can accept one ion for all
83 adsorption systems. This assumption is an obstacle to provide proper interpretations of more
84 complex adsorption mechanisms. The application of reliable models to analyze and explain the
85 adsorption of heavy metal ions on activated carbon surfaces is paramount to develop effective
86 and low-cost water treatment methods.

87 In this research, two homogeneous and heterogeneous models based on statistical
88 physics theory were implemented to explain the adsorption mechanism of Cu²⁺ on a set of
89 activated carbons obtained from different citric wastes namely orange (OP), tangerine (MP),
90 lemon (RLP) and lime (SLP). These models allowed to analyze the adsorption mechanism at
91 the microscopic scale. New insights on steric and energetic parameters that governed the
92 removal of this relevant water pollutant were developed for all tested activated carbons.

93

94 **2. Description of experimental isotherms and statistical physics models**

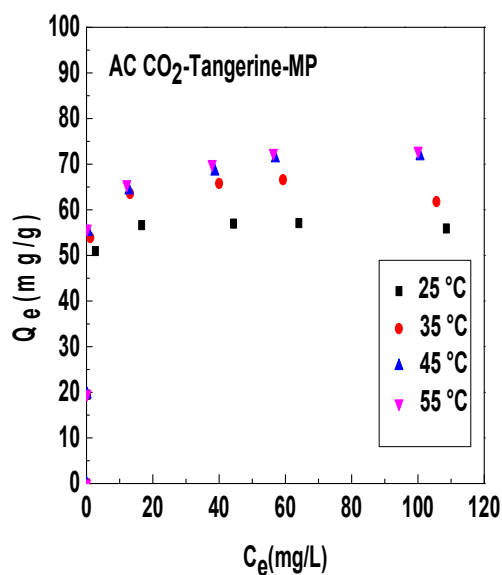
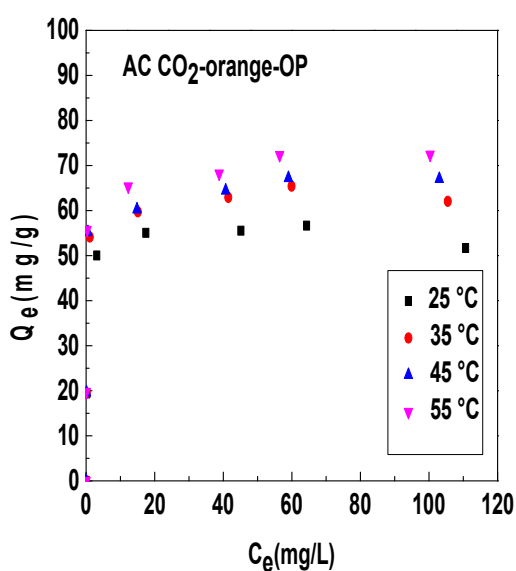
95

96 *2.1. Preparation of AC and quantification of Cu²⁺ adsorption isotherms*

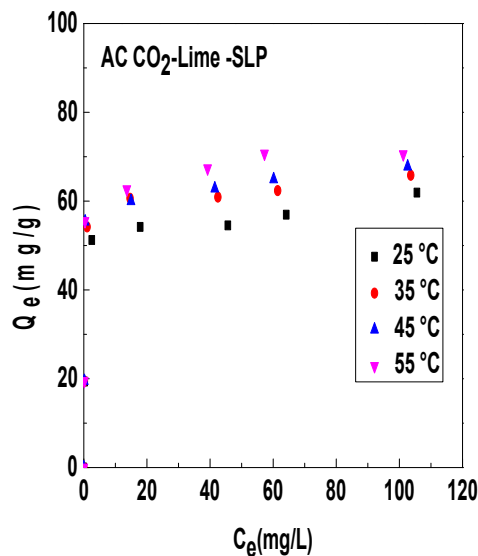
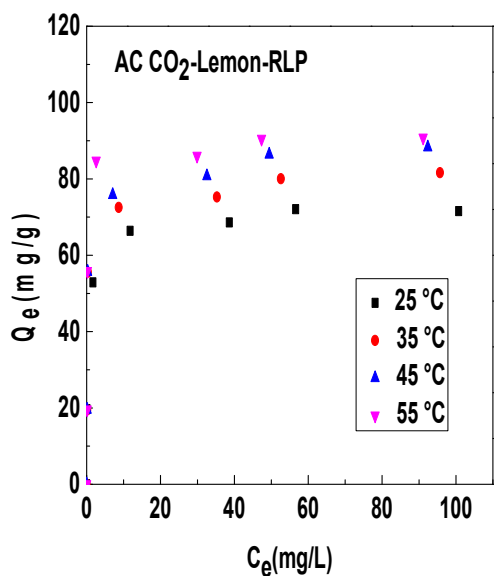
97

98 Cu²⁺ adsorption isotherms were quantified with four activated carbons prepared from citrus
99 waste (Dotto et al. 2011; Perondi et al. 2017). For the adsorbent preparation, 100 g of each citrus

100 waste werelocated in a stainless reactor of 127 x 8.5 cm. The reactor was heated at 5 °C/min
 101 until 900 °C and remained at this temperature for 15 min. Then, the system was cooled until
 102 ambient temperature. All these steps were performed with N₂ flowof 0.2 L/min. Subsequently,
 103 the N₂ flow was replaced by CO₂ flow (2 kg/h for 15 min). Finally, the adsorbent samples were
 104 removed from the reactor, washed and used in adsorption experiments. These adsorbents were
 105 labelled as AC CO₂-orange-OP, AC CO₂-tangerine-OP,AC CO₂-lemon-RLP and AC CO₂-
 106 Lime-SLP.



107



108

109 **Figure 1:** Experimental isotherms of the adsorption of Cu^{2+} ions on different activated carbons
110 at 25-55 °C and pH 5.5.

111

112 Typical batch equilibrium experiments were performed to obtain the Cu^{2+} adsorption
113 isotherms. Aqueous solutions (50 mL) with different initial Cu^{2+} concentrations up to 150 mg/L
114 were prepared from copper sulfate and the solution pH was adjusted to 5.5. Next, these solutions
115 were placed in Erlenmeyer flasks located in a thermostated shaker. Adsorption isotherms were
116 quantified at 25, 35, 45 and 55 °C using an activated carbon dosage of 0.5 g/L under constant
117 stirring of 200 rpm for 5 h. The solid-liquid separation was performed by centrifugation and
118 Cu^{2+} concentration in the liquid was quantified by flame atomic absorption
119 spectroscopy. Then, the equilibrium adsorption capacities were calculated via a mass balance for
120 a stirred tank using the initial and final Cu^{2+} concentrations used in the experiments and the
121 corresponding adsorbent dosage. Figure 1 shows the experimental isotherms of
122 Cu^{2+} adsorption on the four activated carbons analyzed in this paper.

123 Solution temperature positively affected all adsorbed quantities of Cu^{2+} ions on these
124 activated carbons, thus suggesting an endothermic removal process. All experimental isotherms
125 followed the monotonic trend of adsorbed Cu^{2+} quantities as a function of equilibrium
126 concentration until the saturation region was reached. This adsorbent saturation was caused by
127 forming a layer of Cu^{2+} ions adsorbed on the surfaces of tested activated carbons. In this
128 regard, homogeneous and heterogeneous monolayer models developed from statistical physics
129 theory were implemented to analyze Cu^{2+} adsorption isotherms at the microscopic scale. The
130 next two scenarios were tested in this modeling study:

131 **Scenario 1:** A homogeneous monolayer model (HMM) was considered where only one type of
132 functional group participated in the adsorption of Cu^{2+} ions on tested adsorbents. It was assumed
133 that only one adsorption energy was involved in the metal ion removal, which represented the

134 interaction of Cu^{2+} ion-activated carbon surface. The adsorbed quantity calculated with this
135 model is given by (Sellaoui et al. 2018; Dhaouadi et al. 2020c, b, a):

136

137

$$Q_e = \frac{nS_m}{1 + \left(\frac{C_{1/2}}{C_e}\right)^n} \quad (1)$$

138

139 **Scenario 2:** A heterogeneous monolayer model (IMM) was also applied. Two functional
140 groups participated in the adsorption of Cu^{2+} ions with two different adsorption energies: Cu^{2+}
141 ion – adsorption site 1 and Cu^{2+} ion– adsorption site 2. In this model, the adsorbed quantity as a
142 function of the equilibrium concentration is defined as (Dhaouadi et al. 2020b, a, 2021):

143

144

$$Q_e = \frac{n_1 S_{m1}}{1 + \left(\frac{C_1}{C_e}\right)^{n_1}} + \frac{n_2 S_{m2}}{1 + \left(\frac{C_2}{C_e}\right)^{n_2}} \quad (2)$$

145

146 For these models, n and $n_i (i=1, 2)$ are the numbers of Cu^{2+} ions adsorbed per functional group(s),
147 S_m and S_{mi} are the densities of these surface functionalities, $C_{1/2}$ and $C_i (i=1, 2)$ are the
148 concentrations at half-saturation, respectively.

149

150 Characterization results showed that these activated carbons contained different
151 functional groups that can contribute to the adsorption of Cu^{2+} ions. Therefore, these adsorption
152 models were consistent with the surface chemistry of these activated carbons. Note that
153 these models were developed by applying a grand canonical ensemble of statistical physics with
154 the aim of obtaining a better analysis of the adsorption mechanism of this pollutant. Overall,
155 these models assumed that the adsorption of Cu^{2+} ions was a monolayer process, but with the
contribution of one (homogeneous monolayer model) and two (heterogeneous monolayer

156 model) functional groups in the removal of this cation(Dhaouadi et al. 2020b, 2021).In
 157 summary, these models can describe the role of these functional groups on the adsorption of
 158 this metallic ion andcan also characterize the nature of their interactions (i.e., multi-interaction
 159 or multi-ionic process).

160

161

162

163

164

165

166

167

168

169

170 **Table 1:** Results of the Cu²⁺adsorption isothermcorrelation with a homogeneous monolayer
 171 model.

172

173

<i>T</i> (°C)	<i>R</i> ²	<i>n</i>	<i>S_m</i> (mg/g)	<i>C</i> _{1/2} (mg/L)	<i>Q_s</i> (mg/g)
AC CO₂- Orange-OP					
25	0.992	1.13	48.35	0.38	54.63
35	0.994	1.46	42.61	0.31	62.21
45	0.989	1.70	37.88	0.19	64.39
55	0.977	1.82	37.49	0.07	68.23
AC CO₂- Tangerine-MP					

25	0.999	1.07	53.20	0.35	56.92
35	0.995	1.24	51.80	0.32	64.23
45	0.989	1.83	37.65	0.27	68.89
55	0.990	4.20	16.71	0.14	70.18
AC CO₂- Lemon-RLP					
25	0.998	0.63	115.75	0.39	72.92
35	0.987	2.88	26.85	0.25	77.32
45	0.984	2.90	28.55	0.22	82.79
55	0.994	4.55	19.32	0.18	87.90
AC CO₂-Lime-SLP					
25	0.984	1.15	49.55	0.44	56.98
35	0.993	1.56	40.03	0.31	62.44
45	0.988	3.04	20.96	0.238	63.71
55	0.988	3.16	21.42	0.232	67.68

174

175

176

177

178

179

180

181

182

183

184

These models were employed to fit all Cu²⁺ ion adsorption isotherms, and their parameters were determined via a multivariable nonlinear regression with the Levenberg-Marquardt method. Determination coefficients (R^2) and the trends of steric and energetic parameters indicated that the HMM model was the most suitable for analyzing the Cu²⁺ removal at the microscopic scale. Table 1 provides the results of Cu²⁺ adsorption data fitting for the HMM model and their corresponding steric and energetic parameters for tested experimental conditions. In addition, the fitting of Cu²⁺ adsorption isotherms by the HMM model is illustrated in the appendix.

3. Results and discussion

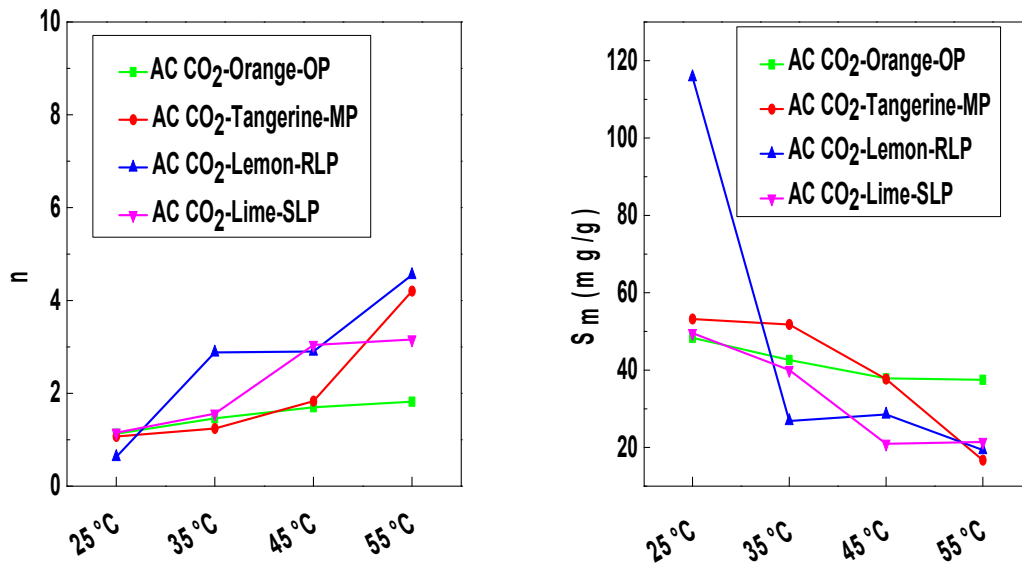
185

186 *3.1. Evaluation of the number of Cu²⁺ ions adsorbed per functional group and their adsorption*
187 *site densities*

188

189 The impact of temperature on the number of adsorbed Cu²⁺ ions per functional group and their
190 corresponding adsorption site densities for these activated carbons is represented in Figure 2.

191 All parameters n were higher than unity except for AC CO₂-Lemon-RLP adsorbent at 25
192 °C. This result indicated that the adsorption of this heavy metal was multi-cationic for these
193 activated carbons, where the functional groups could adsorb several cations
194 simultaneously (Dhaouadi et al. 2020b, a). Indeed, the exceptional case (i.e., $n=0.63$) showed
195 that Cu²⁺ ions could be adsorbed on the surface of AC CO₂-Lemon-RLP via a combined
196 interaction where one and two functional groups can participate in the removal with two
197 different proportions (Dhaouadi et al. 2021). Thermally speaking, the temperature increased the
198 number of Cu²⁺ ions adsorbed per functional group from 1.13 to 1.82, 1.07 to 4.20, 0.63 to 4.59,
199 and 1.15 to 3.16 for the adsorbents AC CO₂-Orange-OP, AC CO₂-Tangerine-MP, AC CO₂-
200 Lemon-RLP and AC CO₂-Lime-SLP, respectively. Overall, these results indicated that the
201 temperature played a relevant role to adsorb the Cu²⁺ ions.



202

203 **Figure 2:** Impact of temperature on the parameters n and S_m for the Cu^{2+} adsorption at pH 5.5
 204 using different activated carbons.

205

206 Figure 2 indicated that the density of functional groups of these activated carbons
 207 reduced as a function of temperature. Moreover, this tendency was inversely proportional to the
 208 number of Cu^{2+} ions adsorbed per functional group. Thus, the increment of the parameter n as a
 209 function of temperature suggested a reduction of the occupied functional groups and,
 210 consequently, a decrement of the adsorption density and vice versa.

211

212 3.2. Performance evaluation of different activated carbons for Cu^{2+} adsorption

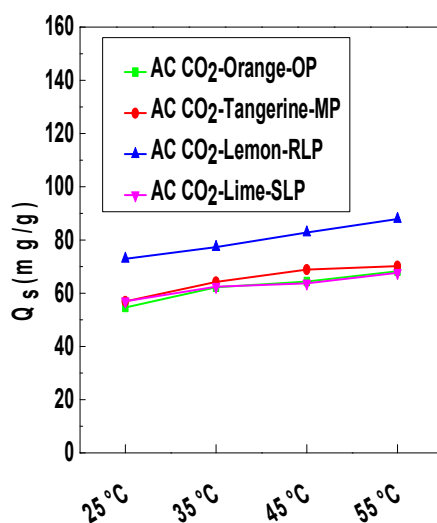
213

214 The performance of tested adsorbents was complemented via the calculation of adsorption
 215 capacities at saturation using the next expression:

216

$$Q_s = nS_m \quad (3)$$

217 The impact of thermal agitation on the adsorbed quantity at saturation Q_s for the different
 218 adsorbents is given in Figure 3.



219

220 **Figure 3:** The adsorbed quantity of Cu²⁺ ions at saturation as a function of temperature for
 221 different activated carbons at pH 5.5.

222

223 Figure 3 indicated that the adsorbed quantity at saturation for the four activated carbons
 224 increased with the solution temperature. This result confirmed that the solution temperature
 225 enhanced the mass transfer phenomena and the diffusion of Cu²⁺ ions inside the porous structure
 226 of these adsorbents. Thus, the increment of this quantity was associated with the number of
 227 adsorbed ions per functional group and the adsorption energy. Comparatively, the AC CO₂-
 228 Lemon-RLP adsorbent showed the highest Cu²⁺ removal and was the most effective for this
 229 purpose. Furthermore, characterization results reported in (Dotto et al. 2011) indicated that
 230 the acidic functionalities of these activated carbons were responsible for Cu²⁺ removal. In
 231 particular, FTIR analysis of activated carbon samples before and after Cu²⁺ adsorption indicated
 232 that the main acidic functional groups were OH and COOH. The absorption bands relative to
 233 these groups presented significant shifts after Cu²⁺ adsorption thus suggesting that OH and
 234 COOH were involved in the interactions with Cu²⁺ ions, and confirming the statistical physics
 235 calculations.

236 For illustration, Table 2 shows the Cu^{2+} adsorption capacities for different activated
 237 carbons reported in the literature. It was clear that these activated carbons can be an alternative
 238 to remove the Cu^{2+} ions from wastewaters and to contribute to the reduction of solid waste
 239 generation. They can also outperform other adsorbents reported in the literature. For instance,
 240 the Cu^{2+} adsorption capacities of 1-iron-modified flaxseed waste, sodium dodecyl sulfate
 241 modified iron pillared montmorillonite, and activated carbons functionalized with magnetic
 242 iron oxide nanoparticles were 7.64, 20.6, and 41.6 mg/g (Li and Wu 2010; Gu et al. 2019;
 243 Cerrahoğlu Kaçakgil and Çetintaş 2021).

244

245 **Table 2.** Cu^{2+} adsorption capacities of activated carbons obtained from different
 246 feedstock (Mariana et al. 2021).

Preparation conditions			
Feedstock	Temperature, °C	Time, min	Adsorption capacity, mg/g
Cauliflower leaves	600	120	75.99
Ginkgo leaf	800	90	310.0
Pinewood sawdust	700	120	419.1

247

248

249 3.3. Cu^{2+} adsorption energy

250

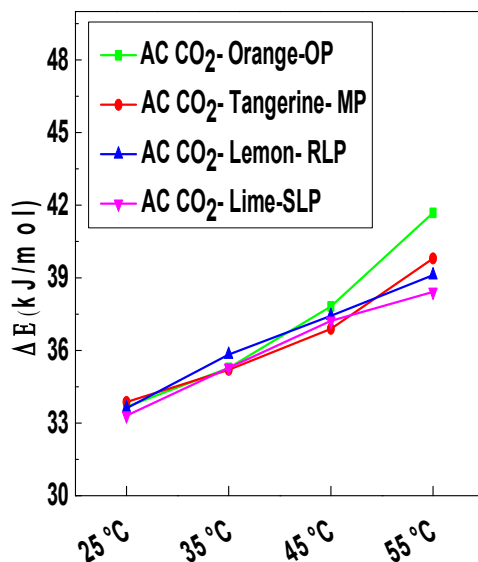
251 Adsorption energy for the interaction Cu^{2+} ion-activated carbon surface was determined from
 252 the concentration values at half-saturation and the following equation (Dhaouadi et al. 2021):

253

$$254 \quad \Delta E_{\text{int}(FG-\text{Cu}^{2+})} = RT \ln \frac{C_s}{C_{1/2}} \quad (4)$$

255

256 where $R=8.314 \text{ J/mol}\cdot\text{K}$ is the ideal gas constant, and C_s is the copper solubility. The adsorption
257 energy for the interaction of acidic functional groups of these activated carbons and Cu^{2+} ions is
258 depicted in Figure 4.



259

260 **Figure 4:** Calculated Cu^{2+} adsorption energies for tested activated carbons.

261

262 All interaction energy values were lower than 40 kJ/mol, thus suggesting that this
263 adsorption process was associated with physical forces. As stated, the acidic functional groups
264 (e.g., OH and COOH) of these activated carbons were involved in the Cu^{2+} adsorption.
265 Furthermore, this adsorption energy increased with solution temperature for all activated
266 carbons.

267

268 4. Conclusions

269

270 A reliable modeling of adsorption data and the corresponding analysis of adsorption
271 mechanism are paramount for the design of water treatment processes effective to remove heavy

272 metals with activated carbons. Therefore, this study reports the statistical physics-based
273 interpretation of Cu^{2+} adsorption using four activated carbons obtained from citrus wastes,
274 which are low-cost feedstock to prepare new adsorbents. Steric and energetic parameters were
275 calculated for the adsorption of this heavy metal using a monolayer adsorption model. Results
276 showed that the Cu^{2+} adsorption was multi-cationic via one functional group (i.e., acidic surface
277 functionalities). In addition, Cu^{2+} adsorption was endothermic and associated with physical
278 interaction forces. At saturation, Cu^{2+} adsorption capacities ranged from 54.6 to 87.9 mg/g for
279 these activated carbons. Finally, this advanced modeling provided interesting interpretations of
280 the adsorption mechanism of this relevant water pollutant with low-cost activated carbons.

281

282 **Acknowledgements**

283

284 Sonia Taamalli, Florent Louis, and Abderrahman El Bakali appreciated the support from the
285 LABEX CaPPA (Chemical and Physical Properties of the Atmosphere), which is funded by the
286 French National Research Agency (ANR) through the PIA
287 (Programmed'Investissement d'Avenir) under contract ANR-11-LABX-0005-01 and also the
288 Regional Council "Hauts de France" and the "European Funds for Regional Economic
289 Development.

290 **-Ethical Approval:** Not applicable

291 **-Consent to Participate:** Not applicable.

292 **-Consent to Publish:** Not applicable.

293 **-Author Contributions: Conceptualization:** Lotfi Sellaoui, Abdemottaleb Ben Lamine,

294 **Methodolog:** Kátia da Boit Martinello, Fatma Dhaouadi, Michael Badawi, Adrián Bonilla-

295 Petriciolet, Luis Felipe Oliveira Silva, Guilherme Luiz Dotto, Sonia Taamalli

296 **Writing - original draft preparation:** LotfiSellaoui, Fatma Dhaouadi, Florent Louis,
297 Abderrahman El Bakali

298 **Supervision:** LotfiSellaoui

299 **-Funding:** Not applicable

300 **-Competing Interests:** The authors declare that they have no competing interests

301 **-Availability of data and materials:** Note applicable

302 **References**

303

304 Anbazhagan S, Thiruvengadam V, Sukeri A (2021) An Amberlite IRA-400 Cl⁻ ion-exchange
305 resin modified with Prosopis juliflora seeds as an efficient Pb²⁺ adsorbent: adsorption,
306 kinetics, thermodynamics, and computational modeling studies by density functional
307 theory. RSC Adv 11:4478–4488. <https://doi.org/10.1039/D0RA10128A>

308 Bell JG, Zhao X, Uygur Y, Thomas KM (2011) Adsorption of Chloroaromatic Models for
309 Dioxins on Porous Carbons: The Influence of Adsorbate Structure and Surface
310 Functional Groups on Surface Interactions and Adsorption Kinetics. J Phys Chem C
311 115:2776–2789. <https://doi.org/10.1021/jp1099893>

312 Cerrahoğlu Kaçakgil E, Çetintaş S (2021) Preparation and characterization of a novel
313 functionalized agricultural waste-based adsorbent for Cu²⁺ removal: Evaluation of
314 adsorption performance using response surface methodology. Sustainable Chemistry
315 and Pharmacy 22:100468. <https://doi.org/10.1016/j.scp.2021.100468>

316 Dhaouadi F, Sellaoui L, Badawi M, Reynel-Ávila H E, Mendoza-Castillo D I, Jaime-Leal J
317 E, Bonilla-Petriciolet A, Lamine A B (2020a) Statistical physics interpretation of the
318 adsorption mechanism of Pb²⁺, Cd²⁺ and Ni²⁺ on chicken feathers. Journal of
319 Molecular Liquids 319:114168. <https://doi.org/10.1016/j.molliq.2020.114168>

320 Dhaouadi F, Sellaoui L, Chávez-González B, Elizabeth Reynel-Ávila H, Diaz-Muñoz L
321 L, Mendoza-Castillo D I, Bonilla-Petriciolet A, Lima E C, Tapia-Picazo J C, Lamine A
322 B (2020b) Application of a heterogeneous physical model for the adsorption of Cd²⁺,
323 Ni²⁺, Zn²⁺ and Cu²⁺ ions on flamboyant pods functionalized with citric acid.
324 Chemical Engineering Journal 127975. <https://doi.org/10.1016/j.cej.2020.127975>

325 Dhaouadi F, Sellaoui L, Dotto GL, Bonilla-Petriciolet A, Erto A, Lamine A B (2020c)
326 Adsorption of methylene blue on comminuted raw avocado seeds: Interpretation of the
327 effect of salts via physical monolayer model. Journal of Molecular Liquids 305:112815.
328 <https://doi.org/10.1016/j.molliq.2020.112815>

329 Dhaouadi F, Sellaoui L, Reynel-Ávila HE, Landín-Sandoval V, Mendoza-Castillo D I, Jaime-
330 Leal J E, Lima E C, Bonilla-Petriciolet A, Lamine A B (2021) Adsorption mechanism
331 of Zn²⁺, Ni²⁺, Cd²⁺, and Cu²⁺ ions by carbon-based adsorbents: interpretation of
332 the adsorption isotherms via physical modelling. Environ Sci Pollut Res.
333 <https://doi.org/10.1007/s11356-021-12832-x>

334 Dotto GL, Vieira MLG, Gonçalves JO, Pinto LA de A (2011) Removal of acid blue 9, food
335 yellow 3 and FD&C yellow no 5 dyes from aqueous solutions using activated
336 carbon, activated earth, diatomaceous earth, chitin and chitosan: equilibrium studies and
337 thermodynamic. Química Nova 34:1193–1199

338 Dou J, Gan D, Huang Q, Chen J, Deng F, Zhu X, Wen Y, Zhang X, Wei Y (2019)
339 Functionalization of carbon nanotubes with chitosan based on MALI multicomponent
340 reaction for Cu²⁺ removal. International Journal of Biological Macromolecules
341 136:476–485. <https://doi.org/10.1016/j.ijbiomac.2019.06.112>

342 Godiya CB, Cheng X, Li D, Chen Z, Lu X (2019) Carboxymethyl cellulose/polyacrylamide
343 composite hydrogel for cascaded treatment/reuse of heavy metal ions in wastewater.

344 Journal of Hazardous Materials 364:28–38.
345 <https://doi.org/10.1016/j.jhazmat.2018.09.076>

346 Gu S-Y, Hsieh C-T, Gandomi YA, Yang Z F, Li L, Fu C C, Juang R S (2019) Functionalization
347 of activated carbons with magnetic Iron oxide nanoparticles for removal of copper ions
348 from aqueous solution. Journal of Molecular Liquids 277:499–505.
349 <https://doi.org/10.1016/j.molliq.2018.12.018>

350 Katiyar R, Patel AK, Nguyen T-B, Singhanian R R, Chen C W, Dong C D(2021) Adsorption of
351 copper (II) in aqueous solution using biochars derived from *Ascophyllum nodosum*
352 seaweed. Bioresource Technology 328:124829.
353 <https://doi.org/10.1016/j.biortech.2021.124829>

354 Kayalvizhi K, Alhaji NMI, Saravanakkumar D, Mohamed S B, Kaviyarasu K, Ayeshamariam
355 A, Al-Mohaimed A M, Abdel Gawwad M R, Elshikh M S (2022) Adsorption of copper and
356 nickel by using sawdust chitosan nanocomposite beads – A kinetic and thermodynamic
357 study. Environmental Research 203:111814.
358 <https://doi.org/10.1016/j.envres.2021.111814>

359 Khan J, Lin S, Nizeyimana JC, Wu Y, Wang Q, Liu X (2021) Removal of copper ions from
360 wastewater via adsorption on modified hematite (α -Fe₂O₃) iron oxide coated sand.
361 Journal of Cleaner Production 319:128687.
362 <https://doi.org/10.1016/j.jclepro.2021.128687>

363 Lam SS, Liew RK, Cheng CK, Rasit N, Ooi C K, Ma N L, Ng J H, Lam W H, Chong C T,
364 Chase H A (2018) Pyrolysis production of fruit peel biochar for potential use in
365 treatment of palm oil mill effluent. Journal of Environmental Management 213:400–
366 408. <https://doi.org/10.1016/j.jenvman.2018.02.092>

367 Lam SS, Liew RK, Lim XY, Ani F N, Jusoha A (2016) Fruit waste as feedstock for recovery
368 by pyrolysis technique. *International Biodeterioration & Biodegradation* 113:325–333.
369 <https://doi.org/10.1016/j.ibiod.2016.02.021>

370 Lemes LFR, Tarley CRT (2021) Combination of supramolecular solvent-based microextraction
371 and ultrasound-assisted extraction for cadmium determination in flaxseed flour by
372 thermospray flame furnace atomic absorption spectrometry. *Food Chemistry*
373 357:129695. <https://doi.org/10.1016/j.foodchem.2021.129695>

374 Li S-Z, Wu P-X (2010) Characterization of sodium dodecyl sulfate modified iron pillared
375 montmorillonite and its application for the removal of aqueous Cu(II) and Co(II).
376 *Journal of Hazardous Materials* 173:62–70.
377 <https://doi.org/10.1016/j.jhazmat.2009.08.047>

378 Mariana M, H.P.S. AK, Mistar EM, Yahya EB, Alfatah T, Danish M, Amayreh M (2021)
379 Recent advances in activated carbon modification techniques for enhanced heavy metal
380 adsorption. *Journal of Water Process Engineering* 43:102221.
381 <https://doi.org/10.1016/j.jwpe.2021.102221>

382 Nyström F, Nordqvist K, Herrmann I, Nordqvist K, Herrmann I, Hedström A, Viklander M
383 (2020) Removal of metals and hydrocarbons from stormwater using coagulation and
384 flocculation. *Water Research* 182:115919.
385 <https://doi.org/10.1016/j.watres.2020.115919>

386 Pan J, Gao Y, Gao B, Guo K, Xu X, Yue Q (2019) One-step synthesis of easily-recoverable
387 carboxylated biogas residues for efficient removal of heavy metal ions from synthetic
388 wastewater. *Journal of Cleaner Production* 240:118264.
389 <https://doi.org/10.1016/j.jclepro.2019.118264>

390 Perondi D, Poletto P, Restelatto D, Manera C, Silva JP, Junges J, Collazzo GC, Dettmer A,
391 Godinho M, Vilela ACF(2017) Steam gasification of poultry litter biochar for bio-
392 syngas production. *Process Safety and Environmental Protection* 109:478–488.
393 <https://doi.org/10.1016/j.psep.2017.04.029>

394 Rukayat OO, Usman MF, Elizabeth OM, Abosede O O, Faith I U (2021) Kinetic Adsorption
395 of Heavy Metal (Copper) On Rubber (*Hevea Brasiliensis*) Leaf Powder. *South African*
396 *Journal of Chemical Engineering* 37:74–80. <https://doi.org/10.1016/j.sajce.2021.04.004>

397 Sellaoui L, Soetaredjo FE, Ismadji S, Benguerba Y, Dotto G L, Bonilla-Petriciolet A, Rodrigues
398 A E, Ben Lamine A, Erto A (2018) Equilibrium study of single and binary adsorption
399 of lead and mercury on bentonite-alginate composite: Experiments and application of
400 two theoretical approaches. *Journal of Molecular Liquids* 253:160–168.
401 <https://doi.org/10.1016/j.molliq.2018.01.056>

402 Sun H, Ji Z, He Y, Wang L, Zhan J, Chen L, Zhao Y (2022) Preparation of PAMAM modified
403 PVDF membrane and its adsorption performance for copper ions. *Environmental*
404 *Research* 204:111943. <https://doi.org/10.1016/j.envres.2021.111943>

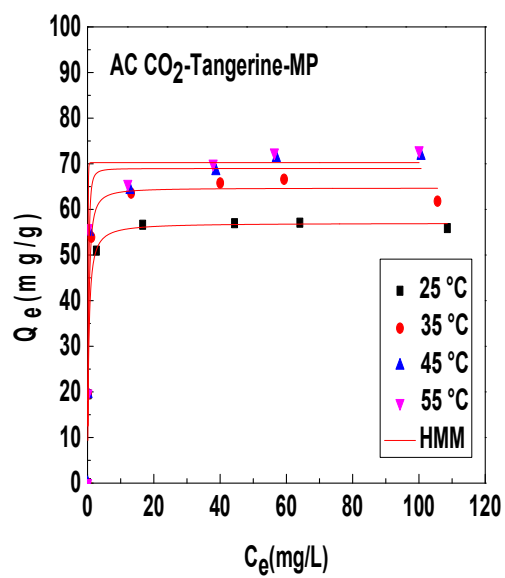
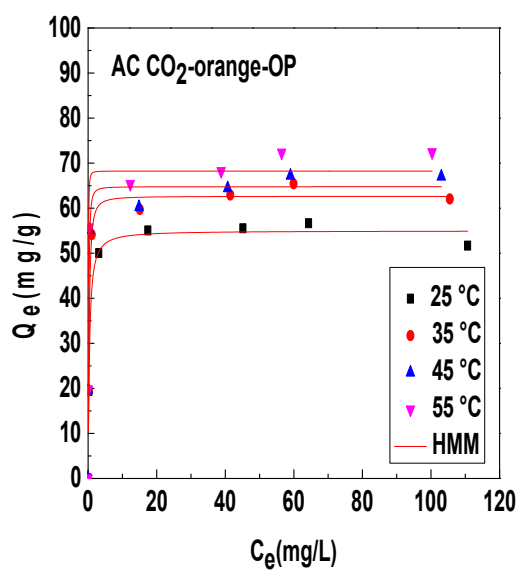
405 Voccianti M, Trofa M, Rodríguez-Estupiñán P, Giraldo L, D’Auria T, Moreno-Piraján J C,
406 Erto A(2014) A rigorous procedure for the design of adsorption units for the removal of
407 cadmium and nickel from process wastewaters. *Journal of Cleaner Production* 77:35–
408 46. <https://doi.org/10.1016/j.jclepro.2013.12.001>

409

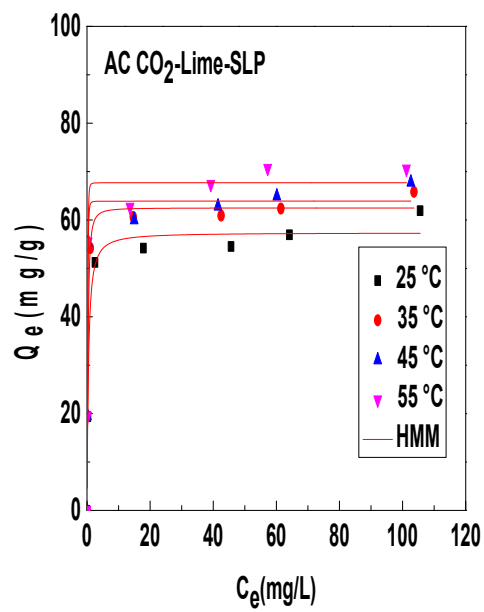
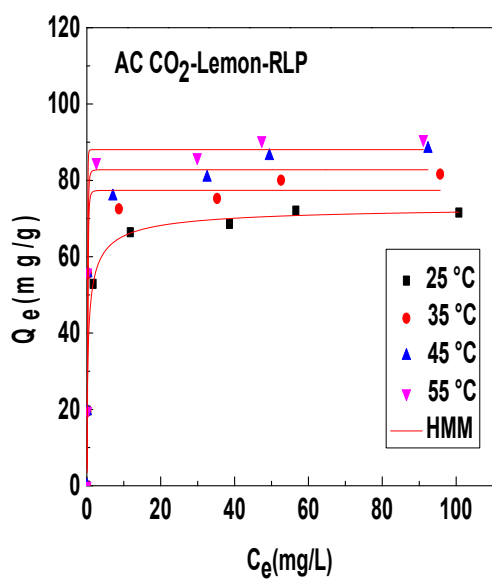
410

411 **Appendix**

412 The fitting data results of the experimental isotherms of Cu^{2+} ions are given below:



413



414

415

416